Lab on a Chip

COMMUNICATION

View Article Online
View Journal

Microfluidic cryofixation for correlative microscopy†

Yara X. Mejia,[a] Holger Feindt,[b] Dongfeng Zhang,[a] Siegfried Steltenkamp[b] and Thomas P. Burg*[a]

Cite this: DOI: 10.1039/c4lc00333k

Received 17th March 2014,
Accepted 30th June 2014

DOI: 10.1039/c4lc00333k

www.rsc.org/loc

Published on 30 June 2014. Downloaded by Max Planck Institut fuer on 15/07/2014 12:09:40.

Cryofixation yields outstanding ultrastructural preservation of cells for electron microscopy, but current methods disrupt live cell imaging. Here we demonstrate a microfluidic approach that enables cryofixation to be performed directly in the light microscope with millisecond time resolution and at atmospheric pressure. This will provide a link between imaging/stimulation of live cells and post-fixation optical, electron, or X-ray microscopy.

Biological microscopy has advanced enormously in recent years through the emergence of optical superresolution techniques, vast improvements in fluorescent proteins and synthetic dyes, and rapid progress in electron and X-ray microscopy. Due to the complementary nature of these methods, there is great interest in being able to image the same specimen by different microscopy techniques.[1–6] However, some microscopy methods require samples to be fixed and processed. For example, in electron microscopy, it is common to prepare thin sections that can be penetrated by the electron beam. Most desirable is a combination whereby live cell imaging before and including the time of fixation can be correlated with ultrastructural studies after fixation. However, in this approach, the time resolution is limited by the fixation technique, which must be fast compared to the process under study. This can be a challenge, as numerous processes that are interesting to observe at high spatial resolution are also very rapid. Unlike imaging science and technology, methods for sample fixation have only evolved incrementally in several decades.

Today, cryofixation is widely considered the gold standard in the preservation of biological ultrastructure down to the molecular scale. This method is almost always preferred over chemical fixation in studies by electron microscopy and electron tomography (EM/ET).[7] The two most common cryofixation methods available are high-pressure freezing (HPF)[8] and plunge freezing.[9] Both differ from slow freezing techniques established for cryopreservation in that samples are flash frozen and the use of cryoprotectants is minimized or eliminated. Plunge-freezing works for samples up to a few microns thick, while HPF is generally used for thicker specimens. With adequate sample preparation, complete vitrification, *i.e.* transformation of liquid water to amorphous ice, is readily achieved by both methods.

Currently, all correlative imaging protocols based on cryofixation require a transfer step from the optical microscope to the HPF or plunging device. Using a commercial rapid transfer system,[5,10] the shortest delay between optical observation and HPF is limited to a few seconds. Moreover, there is a risk of perturbing the sample during transfer. Recent developments have allowed the combination of light stimulation with HPF[11] and plunge-freezing,[12,13] but none of these methods are compatible with live imaging immediately before or during freezing.

Here we demonstrate a microfluidic concept for cryofixation that has high temporal resolution and is compatible with continuous live imaging. The key idea is to set up a steep static temperature gradient between the room temperature sample and a cold reservoir, as illustrated in Fig. 1. This gradient is

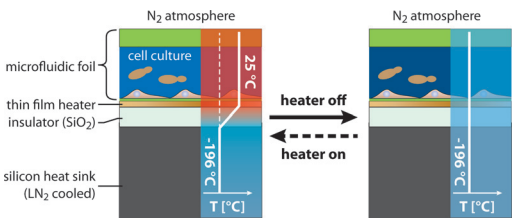

Fig. 1 Cryofixation inside a microfluidic channel. A resistive heater maintains a steep temperature gradient between the room temperature sample and a cold reservoir. When the current is turned off, heat stored in the channel dissipates rapidly, leaving insufficient time for ice crystals to nucleate. The entire process can be observed in the light microscope through the transparent top of the channel (green). A dry nitrogen atmosphere prevents frost formation.

[a] *Max Planck Institute for Biophysical Chemistry, 37077 Goettingen, Germany. E-mail: tburg@mpibpc.mpg.de*
[b] *Micro Systems Technology (MST), Center of Advanced European Studies and Research (caesar), 53175 Bonn, Germany*
† Electronic supporting information (ESI) available. See DOI: 10.1039/c4lc00333k

Published on 30 June 2014. Downloaded by Max Planck Institut fuer on 15/07/2014 12:09:40.

maintained by electrical current flowing through a thin-film resistive heater. When the heater is turned off, the gradient collapses, like the filament in a light bulb cools rapidly when the flow of current is interrupted. Because the power to the heater needs to be continuously dissipated during the warm state, the sample area must be small in order to not exceed the heat sinking capability of the cold reservoir. Here, we limited the size to approximately 0.2 × 2 mm, which is large enough to accommodate a wide range of cell culture systems and some small model organisms.

Microfluidic technology provides an excellent platform for applications that require localized heating and cooling with short time constants. Some examples are briefly outlined in the ESI.† Compared with these studies, the work described here overcomes three key challenges. The first is to approach initial cooling rates of at least ~10^4 °C s^{-1} to suppress ice crystallization. Secondly, the final temperature must be below −140 °C to prevent de-vitrification; and third, continuous flow of fresh media is required during live imaging prior to freezing. These points are addressed in the design by 1) minimizing the thermal mass of the channel containing the sample, 2) minimizing the distance between the cold surface and the sample, and 3) maintaining uninterrupted, room-temperature connections into and out of the heated microchannel. In particular, we found that microfluidic perfusion devices of extremely low thermal mass could be made using microfluidic polymer foils[14] in combination with silicon micromachined components.

Microchannels embedded into PDMS foils only tens of micrometers thick were fabricated by a newly developed process and bonded to silicon fluidic chips, such that the embedded channel was suspended across a dry etched 1 mm circular aperture in the silicon. A detailed description of the microfabricated components and the fabrication steps can be found in Fig. S1 and S2.†

A heated copper frame (Fig. 2) is used to hold and align the fluidic chip containing the PDMS channel with the micro-heater. The assembly is placed on top of the cryogenic stage such that only the heater chip is in direct contact with the cold surface. During operation the micro-heater provides enough power to keep the microchannel at room temperature. The warm copper holder and fluidic chip shield the incoming fluid from the cold temperature of the cryogenic stage, enabling continuous fluid flow through the microchannel while the heater is on (Fig. S3†). The channel is continuously imaged using a 40×/0.6 air objective before, during and after freezing.

In order to evaluate the capabilities of this new cooling technique we carried out finite element simulations (COMSOL). Based on these simulations we have obtained average temperatures and cooling rates as a function of channel height, thickness of the channel bottom, and distance from the bottom of the channel. As seen in the top inset of Fig. 3, the bottom surface of a 15 μm tall channel with a 0.5 μm bottom is able to reach −50 °C in 45 μs and −150 °C in 0.6 ms, resulting in cooling rates of 10^5–10^6 °C s^{-1}. As the distance from the channel bottom increases, the increasing water layer delays the onset of cooling. Nevertheless, the system is still able to cool the entire height of the channel (x = 15 μm) at initial rates of 10^4 °C s^{-1}. Fig. 3 shows a comparison of cooling rates at varying positions from the bottom of the channel for channels 5–60 μm in height and with a thin and a thick bottom layer thickness. As can be seen in this plot, for a thin channel bottom (d = 0.5 μm), water layers of up to 30 μm can be cooled at rates of 10^4 °C s^{-1} or higher, comparable to the average cooling rates obtained with plunge freezing.[15,16] Furthermore, positions close to the bottom of the channel (10 μm or less) result in cooling rates of the order of 10^5 to 10^6 °C s^{-1}, corresponding to the critical cooling rate for pure water.[17,18] Therefore, under ideal conditions, the ultra-rapid microfluidic cooling technique presented here has the potential to greatly reduce or eliminate the need for cryoprotectants. Interestingly, at the same distance from the heater, a channel four times taller (h = 60 μm) results in a rate

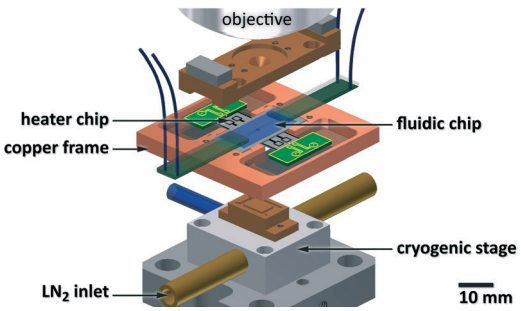

Fig. 2 Assembly of the microfluidic cryofixation device. The channel on the fluidic chip is aligned to the microheater, whose silicon support also serves as a heat sink (see Fig. S2†). A warm copper frame fixes the alignment. Fluid is supplied through two PDMS manifolds with tube connections.

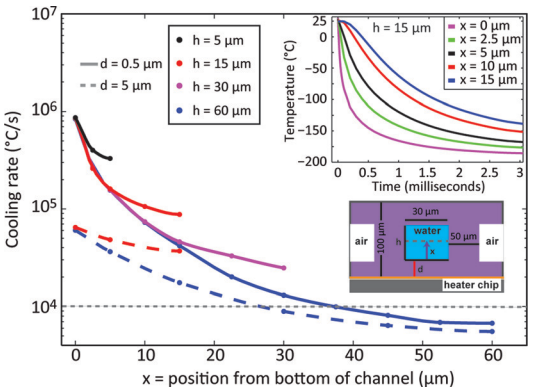

Fig. 3 Simulated cooling rates as a function of position from the bottom of the channel (x) for different channel heights (h) with thin and thick channel bottoms (d). Lateral dimensions similar to the experimental setup (bottom right insert), boundary conditions: −196 °C at the heater chip surface, all others are insulating. Rates are calculated as the time derivative at T = −50 °C, and the dotted line at ~10^4 °C s^{-1} marks the regime typically attained by plunge freezing. (Top inset) Temperature *vs.* time for a 15 μm channel with d = 0.5 μm at different positions from the bottom of the channel.

 This journal is © The Royal Society of Chemistry 2014

Published on 30 June 2014. Downloaded by Max Planck Institut fuer on 15/07/2014 12:09:40.

that is only about half that of a shallower (h = 15 μm) channel. Thus, the cooling rate that a sample experiences depends more strongly on its distance from the cold silicon surface than on how much fluid surrounds it. Due to microfabrication constraints, our first generation cryo-device has a bottom PDMS/parylene layer of around d ~ 5–10 μm. This limits the expected cooling rates close to the bottom of these channels (d = 5 μm in Fig. 3). Yet, these rates should still be high enough to allow for vitrification at low cryoprotectant concentrations.[18,19]

In a first proof-of-principle we used budding yeast as a model system. Yeast cells were grown and resuspended in PM medium containing 800 mM sorbitol as described in the ESI.† The yeast suspension was introduced into a 15 μm tall microchannel and imaged in differential interference contrast (DIC). Initial cooling of the stage after starting the flow of liquid nitrogen resulted in slow frozen channels that looked opaque due to scattering of the light by ice crystals present in the solution (Fig. 4a). In comparison, a channel frozen using our fast freezing technique appears clear, which is evidence for the absence of visible ice crystals.

Fig. 4b demonstrates the ability to carry out fast freezing without compromising real-time optical imaging. In the first three frames, the micro-heater is initially on and the solution is able to flow, allowing the channel contents to be exchanged. When the heater is turned off, the channel cools rapidly, and its content solidifies without visible ice crystals. Due to the fast switching of the electronically regulated current supply, the delay between live optical imaging and fixation is reduced to the time required for the sample to solidify. After cryofixation, the state of the cells immediately prior to freezing can be assessed by means of a wide variety of optical techniques, including bright and dark field, DIC and fluorescence. This method may thereby open many fascinating perspectives for optical cryo-imaging, as outlined briefly in the ESI.†

The rapid transition from a state of unhindered fluid flow to a cryo-immobilized channel is shown in Fig. 4c. Fluorescent beads (1.1 μm in a solution of PBS with 1.4 M sorbitol) were flown through the channel at a high velocity, and streak images were captured at 10 ms intervals. The flow is seen to stop suddenly when the heater is turned off. We are currently working on an exact measurement of the time between switching and solidification of the solution by integrating precision temperature sensors directly on the heated surface for measurements of the cooling curve at high bandwidth.

Fig. S5† shows the thawing process of another channel with visible crystalline ice. Based on the melting of this ice, the initial rate of temperature change is estimated to be between 3×10^3 and 1×10^4 °C s^{-1} for the device shown. Note that this rate is nearly 100 times faster than rates previously available for studies of ice formation using microfluidic or conventional cryo-microscopy systems.[20]

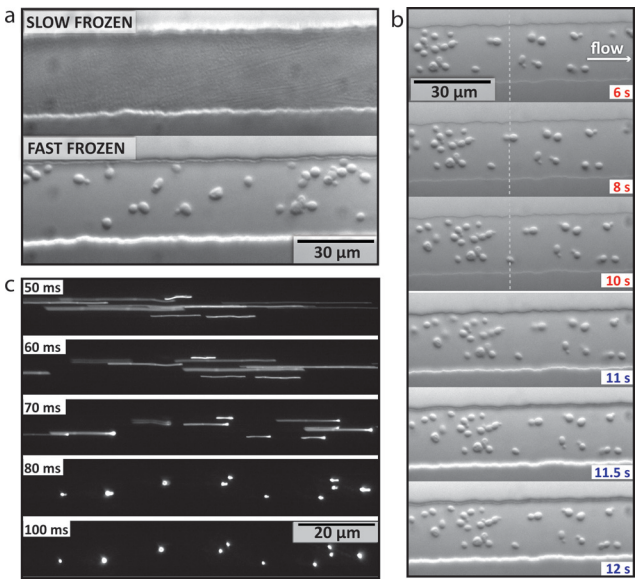

Fig. 4 (a) Slow freezing of a filled microchannel results in the formation of crystalline ice causing the channel to appear opaque. In contrast, a channel frozen with our microfluidic cryofixation method suppressed ice crystal formation, leaving the channel to appear clear. (b) Time sequence of a cryofixation event. In the first three frames, the microheater is on and the yeast cells are moving in the direction of the flow. When the current to the heater is interrupted after t = 10 s, the channel contents are immobilized. Exposure time 10 ms at 0.5 s intervals, DIC image, Andor Clara CCD. (c) A solution of fluorescent beads is flowing through the channel when the heater is turned off. Imaging speed is only limited by the frame rate (here 100 Hz, Andor Neo sCMOS).

Conclusions

We have presented a microfluidic approach to cryofixation of cells by ultra-rapid cooling. The method works at atmospheric pressure and provides uninterrupted visual access to the sample up to and including the time of freezing. As a demonstration of the concept, flowing suspensions of cells and fluorescent microparticles were rapidly frozen directly in the light microscope; sufficient cooling rates were obtained to fully suppress the formation of ice crystals detectable in bright field and DIC. As no sample transfer is required, temporal registration between live imaging and fixation is on the millisecond scale or better.

There are some natural limitations to the approach. Numerical calculations reveal that the finite heat conductivity of water will likely restrict direct vitrification with no cryoprotectants to monolayers of cells less than ~10 μm thick. Samples containing higher concentrations of solutes may be amenable to vitrification up to a thickness of 30–60 μm, compatible with many cell culture models and a few multicellular organisms.[21,22] However, conditions for correct ultrastructure preservation and viability in the microfluidic environment may vary between systems.[23] Furthermore, cryo-transfer tools connecting our device to standard EM protocols, analogous to those routinely done after HPF,[24] need to be developed. Fig. S6† provides an overview on how microfluidic cryofixation can be incorporated into a full correlative light and electron

Published on 30 June 2014. Downloaded by Max Planck Institut fuer on 15/07/2014 12:09:40.

microscopy workflow. Alternatively, techniques based on focused-ion-beam could be used.[25,26]

Within the above boundaries, microfluidic cryofixation should enable a wide range of correlative experiments for studying cellular dynamics, such as membrane trafficking, cell proliferation, synaptic transmission, cell motility, and adhesion. Fast processes could be triggered by optical, electronic or chemical stimuli, stopped by vitrification with millisecond time resolution and observed after cryofixation using conventional and superresolution microscopy (*e.g.* STED), electron, and X-ray imaging. If cells could undergo repeated cycles of vitrification and thawing with minimal disturbances, optical cryo-imaging could be conducted in successive cold periods without sacrificing time resolution, SNR, or field size. Moreover, the method may find applications outside of biology, for example in studying the structure of foams, bubbles, and emulsions by cryo-EM, and in investigating cryoprotection and freezing at rates that far exceed the capabilities of current cryostats.

Acknowledgements

We would like to thank Prof. U.B. Kaupp, Mr. P. Holik, Dr. S. Schmitz, Mr. M. Lacher, and the microsystems technology team at the research center Caesar, and Mr. N. Dudani for his help on finite element simulations. Funding for this work was provided by the Max Planck Society and the Max Planck Institute for Biophysical Chemistry.

References

1 C. Smith, *Nature*, 2012, **492**, 293–297.
2 K. L. McDonald, *J. Microsc.*, 2009, **235**, 273–281.
3 J. M. Plitzko, A. Rigort and A. Leis, *Curr. Opin. Biotechnol.*, 2009, **20**, 83–89.
4 W. Kukulski, M. Schorb, M. Kaksonen and J. A. Briggs, *Cell*, 2012, **150**, 508–520.
5 C. Spiegelhalter, V. Tosch, D. Hentsch, M. Koch, P. Kessler, Y. Schwab and J. Laporte, *PLoS One*, 2010, **5**, e9014.
6 N. Liv, A. C. Zonnevylle, A. C. Narvaez, A. P. Effting, P. W. Voorneveld, M. S. Lucas, J. C. Hardwick, R. A. Wepf, P. Kruit and J. P. Hoogenboom, *PLoS One*, 2013, **8**, e55707.
7 I. Hurbain and M. Sachse, *Biol. Cell*, 2011, **103**, 405–420.
8 U. Riehle and M. Hoechli, *The theory and technique of high pressure freezing*, 1973.
9 D. Glick and B. G. Malmstrom, *Exp. Cell Res.*, 1952, **3**, 125–135.
10 P. Verkade, *J. Microsc.*, 2008, **230**, 317–328.
11 S. Watanabe, B. R. Rost, M. Camacho-Perez, M. W. Davis, B. Sohl-Kielczynski, C. Rosenmund and E. M. Jorgensen, *Nature*, 2013, **504**, 242–247.
12 T. R. Shaikh, D. Barnard, X. Meng and T. Wagenknecht, *J. Struct. Biol.*, 2009, **165**, 184–189.
13 Z. H. Lu, T. R. Shaikh, D. Barnard, X. Meng, H. Mohamed, A. Yassin, C. A. Mannella, R. K. Agrawal, T. M. Lu and T. Wagenknecht, *J. Struct. Biol.*, 2009, **168**, 388–395.
14 M. Focke, D. Kosse, C. Muller, H. Reinecke, R. Zengerle and F. von Stetten, *Lab Chip*, 2010, **10**, 1365–1386.
15 P. Echlin, *Low-Temperature Microscopy and Analysis*, 1992.
16 J. C. Gilkey and L. A. Staehelin, *J. Electron Microsc. Tech.*, 1986, **3**, 177–210.
17 M. Warkentin, V. Stanislavskaia, K. Hammes and R. E. Thorne, *J. Appl. Crystallogr.*, 2008, **41**, 791–797.
18 M. Warkentin, J. P. Sethna and R. E. Thorne, *Phys. Rev. Lett.*, 2013, **110**, 015703.
19 V. Berejnov, N. S. Husseini, O. A. Alsaied and R. E. Thorne, *J. Appl. Crystallogr.*, 2006, **39**, 244–251.
20 C. A. Stan, G. F. Schneider, S. S. Shevkoplyas, M. Hashimoto, M. Ibanescu, B. J. Wiley and G. M. Whitesides, *Lab Chip*, 2009, **9**, 2293–2305.
21 J. El-Ali, P. K. Sorger and K. F. Jensen, *Nature*, 2006, **442**, 403–411.
22 K. Chung, M. M. Crane and H. Lu, *Nat. Methods*, 2008, **5**, 637–643.
23 L. Kim, Y. C. Toh, J. Voldman and H. Yu, *Lab Chip*, 2007, **7**, 681–694.
24 J. E. Kuo, *Electron Microscopy- Methods and Protocols*, 2007.
25 K. Narayan, C. M. Danielson, K. Lagarec, B. C. Lowekamp, P. Coffman, A. Laquerre, M. W. Phaneuf, T. J. Hope and S. Subramaniam, *J. Struct. Biol.*, 2014, **185**, 278–284.
26 K. Wang, K. Strunk, G. P. Zhao, J. L. Gray and P. J. Zhang, *J. Struct. Biol.*, 2012, **180**, 318–326.

 This journal is © The Royal Society of Chemistry 2014